LWT - Food Science and Technology 253 (2026) 119663

Contents lists available at ScienceDirect

LWT

journal homepage: www.elsevier.com/locate/lwt

Engineering a single protein molecules bio-iridium oxide nanozyme for colorimetric evaluation of total antioxidant capacity in food samples

Shuangshuang Yan [a,d,1], Dongying An [a,c,1], Yutian Zhou [a,c,1], Xinli Guo [a,c], Zhihang Qin [c], Fangliang Yang [a,*], Yang Zhang [a,b,**]

[a] Shenyang Key Laboratory of Medical Molecular Theranostic Probes in School of Pharmacy, Shenyang Medical College, 146 Huanghe North Avenue, Shenyang, 110034, China
[b] Liaoning Province Key Laboratory for Phenomics of Human Ethnic Specificity and Critical Illness, Shenyang Medical College, 146 Huanghe North Avenue, Shenyang, 110034, China
[c] School of Basic Medicine, Shenyang Medical College, 146 Huanghe North Avenue, Shenyang, 110034, China
[d] School of Public Health, Shenyang Medical College, 146 Huanghe North Avenue, Shenyang, 110034, China

ARTICLE INFO

Keywords:
Food analysis
Total antioxidant capacity
Nanozyme
Sensor

ABSTRACT

Antioxidants play a critical role in scavenging free radicals to prevent oxidative damage, underscoring the importance of evaluating the antioxidant content in various consumables. A novel colorimetric method utilizing iridium oxide (IrOx) nanozymes was developed to quantify the total antioxidant capacity (TAC) of food samples. By employing bovine serum albumin (BSA) as a structural template and iridium as the precursor, a biomimetic mineralization approach was employed to synthesize b-IrOx nanozymes with intrinsic peroxidase-like activity. These nanozymes effectively mimic natural peroxidases in catalyzing redox reactions. Through single electron transfer (SET) and hydrogen atom transfer (HAT) mechanisms, antioxidants in samples can outcompete substrates for •OH, leading to a color change dependent on antioxidant concentration. The proposed b-IrOx-based colorimetric assay accurately determined the TAC of mango juice (948.31 ± 0.83 μM), yellow peach juice (776.72 ± 2.47 μM), and apple juice (154.77 ± 1.70 μM) with high precision (recovery rate: 90.49%-110.62%) and reproducibility (RSD<3.0%). Comparison with a commercial TAC standard kit validated the reliability of the TMB colorimetric assay using b-IrOx nanozymes, showing no significant statistical difference between the two methods ($p > 0.05$). Thus, the b-IrOx colorimetric assay presents a cost-effective and straightforward approach for rapid and accurate TAC determination in food samples.

1. Introduction

Antioxidants serve as a critical component of the body's metabolic defense system, effectively protecting against oxidative stress and damage caused by free radicals (Demirci-Çekiç et al., 2022; Forman & Zhang, 2021; Zhang et al., 2021; Chaudhary et al., 2023a). The human body produces only a small number of antioxidants on its own, so most antioxidants need to be obtained from outside sources, with diet being the main and richest source of these external antioxidants (Çelik et al., 2024). Recent research shows that consuming foods rich in antioxidants is crucial for preventing heart disease, cancer, and neurodegenerative diseases (Jelic et al., 2021; Teleanu et al., 2022; Velusamy et al., 2020). Total antioxidant capacity (TAC) serves as a key indicator for evaluating the combined activity of all antioxidants present in food and biological systems, as it directly reflects the overall antioxidant ability (Han et al., 2022; Possa et al., 2021; Sánchez-Martín et al., 2022). Therefore, accurately detecting TAC in food is highly important for assessing the nutritional value of food products and maintaining quality control throughout food processing (Apak et al., 2016).

Up to now, several analytical techniques have been explored for TAC determination, including the use of 2,2′-azino-bis(3-ethylbenzo thiazoline-6-sulfonic acid) (ABTS) assay, ferric reducing antioxidant

* Corresponding author.
** Corresponding author. Shenyang Key Laboratory of Medical Molecular Theranostic Probes in School of Pharmacy, Shenyang Medical College, 146 Huanghe North Avenue, Shenyang, 110034, China.
E-mail addresses: yangfangliang@symc.edu.cn (F. Yang), zhangyang@symc.edu.cn (Y. Zhang).
[1] These authors contributed equally to this work.

https://doi.org/10.1016/j.lwt.2026.119663
Received 17 March 2026; Received in revised form 17 June 2026; Accepted 22 June 2026
Available online 25 June 2026
0023-6438/© 2026 The Authors. Published by Elsevier Ltd. This is an open access article under the CC BY license (http://creativecommons.org/licenses/by/4.0/).

power (FRAP) assay, and 2,2-diphenyl-1-picrylhydrazyl (DPPH) assay (Egu et al., 2022; Li et al., 2021; Munteanu & Apetrei, 2021; Rumpf et al., 2023). These methods construct colorimetric or fluorescent detection systems to quantify TAC by relying on single electron transfer (SET) and hydrogen atom transfer (HAT) as their core reaction mechanisms (Nakano et al., 2019; Zeb, 2020). However, these classic methods suffer from certain application limitations due to inherent drawbacks of their reaction mechanisms: the DPPH assay relies on a combination of radical single electron transfer and partial hydrogen atom transfer for colorimetric detection, but the DPPH radical is only soluble in organic solvents and is photosensitive and easily decomposed, making it unsuitable for measuring aqueous fruit and vegetable samples; the ABTS assay, based on the single electron transfer mechanism, requires pre-chemical oxidation to generate the cationic radical, which has poor storage stability; the FRAP assay operates only under strongly acidic conditions through the single electron reduction pathway of Fe^{3+}, thus failing to recognize antioxidant components such as polyphenols and flavonoids that exert activity via hydrogen atom transfer, leading to underestimation of the true antioxidant capacity of samples. Moreover, commercial kits generally employ natural peroxidase as the catalytic core, which suffers from high detection cost and stringent storage conditions (Alshatteri et al., 2023; Li et al., 2025; Niu et al., 2024). In addition, instrumental analytical techniques including high performance liquid chromatography (HPLC) (Yalçın et al., 2021a), gas chromatography (Duarte et al., 2023), and electrochemical analysis (Ishida et al., 2022) have also been widely used for TAC determination. Although these techniques may be well applicable for TAC assays, most of them suffer from obvious disadvantages such as expensive equipment, time-consuming experimental processes, the requirement for highly specialized skills, and dependence on specific reaction conditions (Acidri et al., 2020). Therefore, there is an urgent need to develop a simple, convenient, and rapid alternative method for TAC determination to fulfill the demands of widespread practical applications in food science and related fields.

Nanozymes, which possess inherent enzyme-like catalytic properties, have gained significant interest in recent years because they offer benefits compared to natural enzymes, including lower production costs, greater stability in various environments, and ease of large-scale manufacturing (Yang et al., 2021b; Liang & Yan, 2019; Mou et al., 2022). Colometry offers a solution to current technological constraints in antioxidant analysis due to its cost-effectiveness, simplicity, and faster analysis time (Chen et al., 2023b; Deshwal et al., 2024; Baranwal et al., 2024). For 3,3′,5,5′-tetramethylbenzidine (TMB)-based colorimetric TAC detection, the typical reaction principle is as follows: in the presence of H_2O_2, a catalyst can promote the oxidation of the chromogenic substrate TMB, resulting in its transformation from a colorless state to a blue oxidized product (oxTMB). In the presence of antioxidants within the system, these compounds compete with TMB for the hydroxyl radicals (•OH) produced during the reaction. This competitive interaction inhibits the formation of oxidized TMB, resulting in a reduction in the intensity of the blue signal. This alteration in the signal exhibits a positive correlation with the concentration of antioxidants, thereby serving as the fundamental principle for the quantification of TAC (Chen et al., 2025). In conventional TMB colorimetric TAC assays, natural peroxidase is typically used as catalyst, but its poor stability and high cost limit practical use. Therefore, developing a highly stable and easy-to-synthesize nanozyme with excellent POD-like activity is highly desired to replace natural enzymes for reliable TAC detection in complex food matrices (Zhang et al., 2024).

In this study, we developed a bovine serum albumin (BSA)-templated iridium oxide nanozyme (b-IrOx)-based colorimetric sensor for the sensitive determination of TAC in food samples. The b-IrOx nanozyme exhibits POD-like activity, catalyzing the oxidation of the chromogenic substrate TMB in the presence of H_2O_2 to generate blue-colored oxidized TMB (oxTMB). In the presence of antioxidants, such as those found in food samples, the antioxidants scavenge hydroxyl radicals (•OH) through HAT and single electron transfer SET mechanisms. This competition with TMB for reactive oxygen species results in a concentration-dependent decrease in the colorimetric signal. By leveraging this competitive inhibition principle, we established a colorimetric assay for TAC determination in three types of commercial fruit juices. The results validate the reliability and feasibility of the b-IrOx-based sensor for practical food sample analysis. This study presents a stable and reliable nanozyme-based colorimetric platform for TAC assessment, offering broad application potential in future food quality monitoring endeavors.

2. Materials and methods

2.1. Reagents and chemicals

Iridium (III) chloride, 6-Hydroxy-2,5,7,8-tetramethylchroman-2-carboxylic acid (Trolox), and 3,3′,5,5′-tetramethyl-benzidine (TMB) were purchased from Yuanye Bio-Technology Co., Ltd. (Shanghai, China). Bovine serum albumin (BSA) was purchased from Labgic Technology Co., Ltd. (Beijing, China). Glutathione (GSH), cysteine (Cys), gallic acid (GA), caffeic acid (CA), and terephthalic acid (TA) were purchased from Aladdin Biochemical Technology Co., Ltd. (Shanghai, China). Ascorbic acid (AA) and other reagents were purchased from Sinopharm Chemical Reagent Co., Ltd. (Shanghai, China). The total antioxidant capacity assay kits (ABTS method and FRAP method) was purchased from Beyotime Biotechnology Co., Ltd. (Shanghai, China).

2.2. Apparatus

Fourier transform infrared (FTIR) spectroscopy measurements were conducted using a Nicolet 6700 spectrometer (Thermo Nicolet Corporation, USA) with a wavenumber range of 400–4000 cm^{-1}. X-ray photoelectron spectroscopy (XPS) data were acquired using a Thermo Scientific ESCALAB 250Xi spectrometer. Morphological and microstructural analyses were performed using a high-resolution transmission electron microscope (HRTEM, FEI Tecnai G2 F30) and a scanning electron microscope (SEM, Hitachi SU8010). Ultraviolet-visible (UV-vis) spectroscopic analysis was carried out using a PERSEE F-7000 UV-vis spectrophotometer and a BioTek CYTATION 5 Microplate Reader. Fluorescence analysis was performed using a fluorescence spectrophotometer F-7000 (Hitachi, Japan).

2.3. Synthesis of b-IrOx nanozymes

In this work, the b-IrOx with POD-like activity was synthesized through a biomineralization process under alkaline conditions. BSA (150 mg) was dissolved in 10 mL of deionized water. Subsequently, an aqueous solution of Iridium(III) chloride (4 mL, 25 mM) was added dropwise to the BSA solution. The mixture was stirred continuously for 30 min, followed by the addition of 2 M NaOH solution to adjust the pH to 12.0. The reaction was allowed to proceed for 24 h at 80 °C with vigorous stirring. The resulting product was collected, washed three times alternately with ethanol and deionized water, and then centrifuged at 10000 rpm for 10 min. The collected product was then freeze-dried and stored at 4°C for further use.

2.4. POD-like activity of b-IrOx nanozymes

The POD-like activity of b-IrOx was assessed by its catalytic oxidation of TMB in the presence of H_2O_2, which results in the formation of blue oxTMB. The experimental protocol entailed the sequential addition of 30 μL of TMB (1 mM), 30 μL of b-IrOx (50 μg/mL), and 30 μL of H_2O_2 (5 mM) solutions, with the total volume adjusted to 600 μL using a NaAc-HAc buffer (pH 4.0). After incubating the mixture at room temperature for 30 min, UV-visible spectra were measured over the wavelength range of 450–750 nm. To optimize the catalytic efficiency,

several key parameters of the catalytic reaction were investigated, including pH (3.0-10.0), temperature (0-60 °C), b-IrOx concentration (5-250 μg/mL), and catalytic reaction time (1-60 min).

2.5. Research on kinetics

Steady-state kinetic experiments were performed to evaluate the POD-like catalytic behavior of b-IrOx nanozymes, using TMB and H_2O_2 as the oxidant. All experiments were conducted under the optimized reaction conditions (pH 4.0, 25 °C, 50 μg/mL of b-IrOx concentration) to ensure consistency and reliability. The *Michaelis-Menten* equation (Eq. (1)) was used to the substrate concentration (*[S]*)-initial reaction velocity (*V*) data, and the *Lineweaver-Burk* double reciprocal plot was applied for verification. Kinetic assays with variable TMB and H_2O_2 concentration and kinetic parameter calculation were provided in the Supplementary Information.

2.6. Detection of antioxidants and establishment of TAC quantification method

To detect target antioxidants and quantify TAC, a unified TMB-based colorimetric biosensing system using b-IrOx nanozyme was adopted. The analytes included three individual antioxidants (AA, caffeic acid, and GSH) and Trolox, which served as the standard for TAC quantification. For TAC quantification, a series of standard aqueous solutions of Trolox were prepared to construct the standard curve for TAC quantification. For the TMB-based system, 30 μL of antioxidants with gradient concentrations, including Trolox (0.1-100 μM), AA (0.5-20 μM), caffeic acid (0.1-40 μM), and GSH (0.2-90 μM) standard solution, 30 μL of b-IrOx nanozyme solution (50 μg/mL), 30 μL of H_2O_2 solution (5 mM) and 30 μL of TMB chromogenic solution (1 mM) were mixed sequentially. The total volume was adjusted to 600 μL using NaAc-Hac buffer (pH 4.0). After incubation at 25°C for 30 min, the absorbance at wavelength range of 500-750 nm was measured. All results are presented as mean ± SD (n = 3). A standard curve was plotted with the absorbance decrease value as the ordinate and Trolox concentration as the abscissa, and a regression equation was established to quantify the TAC in samples. The TAC of samples was expressed as Trolox equivalent concentration.

2.7. Selectivity assay

To evaluate the selectivity of the b-IrOx-based sensing method for antioxidants, interference experiments were conducted using common interfering substances in fruit juices (glucose, amino acids, metal ions) and various antioxidants (AA, GA, CA, GSH, Cys). The reaction system for TMB-based assay contained 50 μg/mL b-IrOx, 1 mM TMB, 5 mM H_2O_2, and pH 4.0 buffer. Interfering substances were introduced at concentrations of 20 μM for glucose and amino acids, or 100 μM for metal ions, while antioxidants were added at a concentration of 10 μM. The TMB-based system was incubated at room temperature for 30 min with absorbance measured at 652 nm.

2.8. Sample treatment and validation assay

Three types of commercially available non-concentrated reduced (NFC) juices (mango juice, yellow peach juice, and apple juice) from popular brands in supermarkets were selected as samples to assess the accuracy and practical applicability of the established b-IrOx-based sensing method.

The NFC juice samples were first mixed thoroughly to ensure homogeneity, and then directly analyzed using the sensing system. Their TAC was determined via three approaches for cross-validation: 1) the b-IrOx-based TMB colorimetric assay; 2) a commercially available standard TAC assay kit (ABTS and FRAP methods), where the detection was performed strictly according to the kit instruction manual to obtain the reference TAC values of the fruit juice samples. These two approaches were designed to verify the reliability of the self-established b-IrOx system against mature commercial detection tools. The test results were reported as the mean ± SD of three independent parallel measurements. In cases where the sample contained a higher concentration of antioxidants than the linear range of the Trolox standard curve (0.1-100 μM Trolox equivalent), it was further diluted with deionized water. The TAC of the original NFC juice sample (*T, μM*) was calculated using formula (1):

$$T = C_{Trolox} \times \frac{V_{total}}{V_{sample}} \times D \quad (1)$$

Where: C_{Trolox} is Trolox equivalent concentration of the diluted sample, obtained from the standard curve (μM); V_{total} is total volume of the detection reaction system (μL, 200 μL in this work); V_{sample} is volume of the diluted sample added to the reaction system (μL, 10 μL in this work); D is dilution ratio of the original NFC juice.

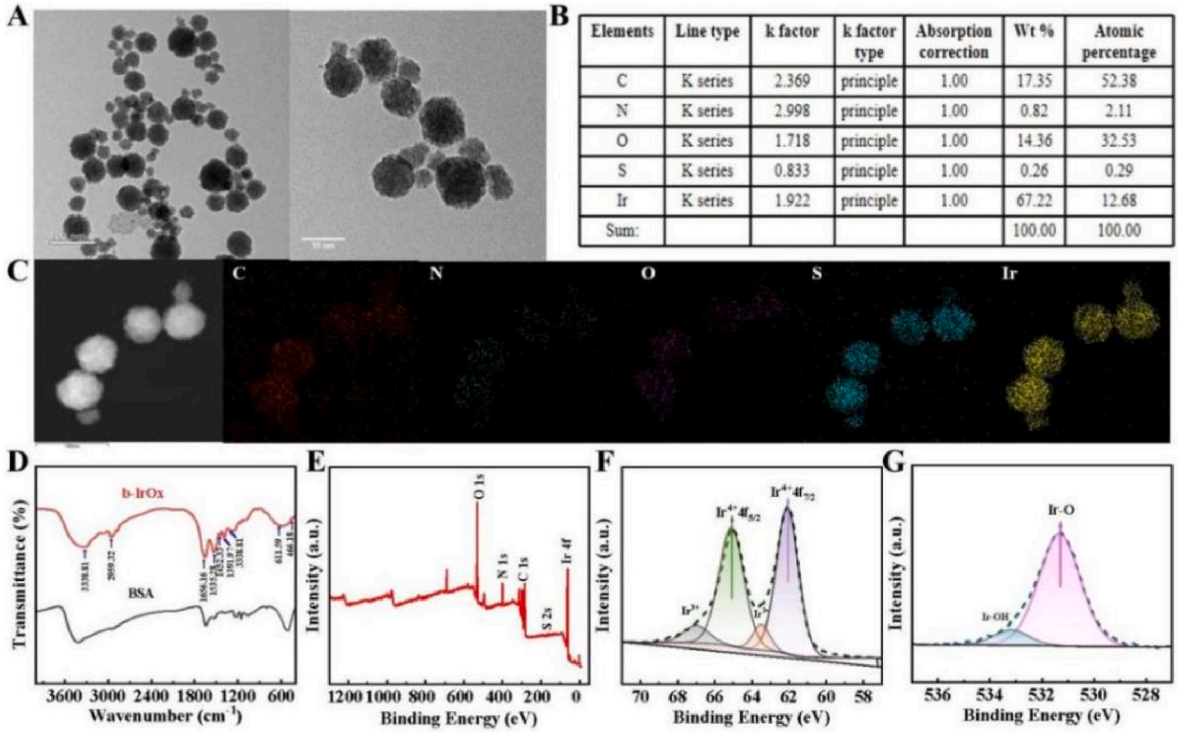
3. Results and discussion

3.1. Synthesis and characteristics of b-IrOx

In this study, biomineralization of b-IrOx nanoparticles commenced with the adsorption of Ir^{3+} ions onto BSA, facilitated by the carboxy and amino groups' affinity towards metal ions. The TEM images of b-IrOx nanoparticles exhibited a spherical morphology as shown in Fig. 1A, with an average diameter of 34.56 nm. The elemental analysis of b-IrOx nanoparticles in Fig. 1B and C clearly identified the presence of Ir, C, N, S, and O elements, which aligns with the composition of BSA and IrOx. Additionally, the elemental mapping images Fig. 1C showed that these elements are evenly distributed throughout the nanoparticles, confirming that BSA has been effectively combined with the IrOx core to create b-IrOx. As shown in Fig. 1D, the characteristic peaks of b-IrOx corresponding to functional groups of BSA were existed, and subtle shifts in partial peak positions indicated interactions between BSA and IrOx, confirming the integration of the two components. XPS was employed to analyze the surface chemical state of b-IrOx nanoparticles. In Fig. 1E, the XPS full spectrum confirmed the presence of Ir, C, N, O, and S elements on the nanoparticle surface, aligning with EDS results and ruling out significant contamination from other elements. In Fig. 1F, the high-resolution Ir 4f XPS spectrum showed distinct spin-orbit splitting peaks. The peaks observed at 61.8 eV and 64.7 eV correspond to the $4f_{7/2}$ and $4f_{5/2}$ states of Ir^{4+}, respectively, providing direct evidence that iridium in the nanoparticles predominantly exists in the +4 oxidation state. The deconvolution of the high-resolution O 1s spectrum Fig. 1G identified two principal peaks: one located at 532.6 eV, which is ascribed to the -COOH and -C=O functional groups originating from bovine serum albumin (BSA), and another at 531.0 eV, corresponding to Ir-O bonds characteristic of IrO_2. This result further confirmed the formation of IrO_2-related species in the b-IrOx nanoparticles, completing the characterization of their surface chemical structure. Taken together, the comprehensive characterizations collectively confirmed the successful synthesis of b-IrOx nanoparticles with well-defined spherical morphology, uniform BSA combination, and dominant Ir^{4+} oxidation state within IrO_2-related species, providing a comprehensive structural basis for exploring their functional properties in subsequent studies.

3.2. POD-like activity of b-IrOx

For the purpose of examining the enzyme-mimetic properties of the prepared b-IrOx, the oxidation reaction of TMB chromogenic substrate was carried out in the presence of b-IrOx and H_2O_2 by using a UV-vis spectrophotometer to monitor the formation of oxidized products. As shown in Fig. 2A, the conversion of TMB substrate to oxTMB was monitored at λ_{max} = 652 nm. The results confirm the generation of oxTMB product, demonstrating the POD-like catalytic activity of b-IrOx



Elements	Line type	k factor	k factor type	Absorption correction	Wt %	Atomic percentage
C	K series	2.369	principle	1.00	17.35	52.38
N	K series	2.998	principle	1.00	0.82	2.11
O	K series	1.718	principle	1.00	14.36	32.53
S	K series	0.833	principle	1.00	0.26	0.29
Ir	K series	1.922	principle	1.00	67.22	12.68
Sum:					100.00	100.00

Fig. 1. Characterization of b-IrOx nanoparticles (A), TEM images (B), EDS analysis. (C), Elemental mapping images (D), FT-IR spectra of BSA and b-IrOx (E), XPS full-spectrum of b-IrOx (F), High-resolution Ir 4f XPS spectrum of b-IrOx nanoparticles (G), High-resolution O 1s XPS spectrum of b-IrOx nanoparticles.

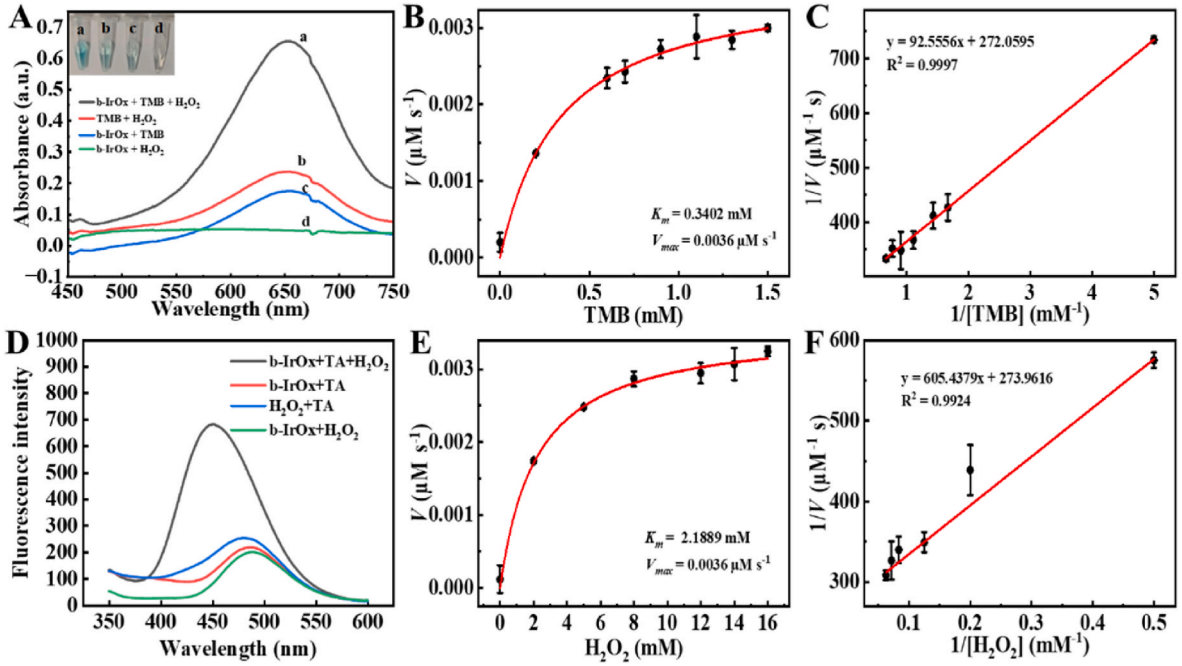


Fig. 2. (A), POD-like activity: typical absorption spectra of TMB, oxidation catalyzed by b-IrOx and control groups in the presence of H_2O_2 at pH 4.0 (B), The concentration of H_2O_2 was 5 mM and the TMB concentration varied (C), Double reciprocal plots of the *Michaelis-Menten* equation from the activity date of the concentration of TMB (D), Fluorescent spectra of TA after reaction with H_2O_2 in the absence and presence of b-IrOx. Concentration of b-IrOx was 50 μg/mL, H_2O_2 was 10 mM (E), The concentration of TMB was 1 mM and the H_2O_2 concentration varied (F), Double reciprocal plots of the *Michaelis-Menten* equation from the activity date of the concentration of H_2O_2.

towards TMB, accompanied by a significant colorimetric response.

To elucidate the primary factors influencing TMB oxidation, various operational parameters were assessed, including b-IrOx concentration, reaction time, temperature, and pH. In the TMB system, as shown in Fig. S1A, the catalytic activity of b-IrOx increases from pH 3.0 to 10.0, peaking at pH 4.0, and then sharply decreases under weakly acidic and neutral conditions. Subsequent experiments used acetic acid buffer at pH 4.0. The effect of reaction temperature Fig. S1B shows that the

catalytic activity of b-IrOx significantly increases from 10°C to 60°C; however, considering the limitation of high temperature on practical application scenarios, 25 °C was selected as the optimal reaction temperature. Furthermore, the concentration and incubation time (1-60 min) were investigated for its impact on UV signal under the optimal pH and temperature conditions. b-IrOx concentration optimization Fig. S2A demonstrated that the catalytic activity increased with the nanozyme concentration from 5 to 250 μg/mL. To balance catalytic efficiency and practical considerations, 50 μg/mL was determined as the optimal b-IrOx concentration for all subsequent experiments. As shown in Fig. S2B, the UV signal significantly increases from 1.0 to 30 min and gradually stabilizes. For experimental convenience, the incubation time was 30 min.

To quantitatively assess the POD-like activity of b-IrOx, steady-state kinetics were studied by independently varying the concentrations of H_2O_2 or TMB. For the TMB substrate system, when H_2O_2 was fixed, the *Michaelis-Menten* curve for TMB and its corresponding *Lineweaver-Burk* plot Fig. 2B and C yielded $K_m = 0.34$ mM and $V_{max} = 0.36 \times 10^{-8}$ M/s. When TMB was fixed, the *Michaelis-Menten* curve for H_2O_2 and its corresponding *Lineweaver-Burk* plot Fig. 2E and F gave $K_m = 2.19$ mM and $V_{max} = 0.36 \times 10^{-8}$ M/s. Notably, high affinity of b-IrOx for H_2O_2 not only boosts its catalytic performance but also supports the upcoming sensitive TAC colorimetric assay.

The mechanism of the b-IrOx nanozyme-based colorimetric method involves a competitive reaction between TMB and antioxidants for •OH on nanozymes. To confirm •OH generation, TA reacts with •OH to form fluorescent 2-hydroxy terephthalic acid (TAOH). As shown in Fig. 2D, a strong fluorescent signal at 430 nm was observed in the IrOx + TA + H_2O_2 group, while control groups (IrOx + TA, H_2O_2 + TA, IrOx + H_2O_2) had weak or no fluorescence. It is demonstrated that b-IrOx catalyzes H_2O_2 to generate •OH, enabling SET and HAT reactions for the detection of antioxidants.

3.3. b-IrOx-based colorimetric methods for antioxidants

Under the optimal conditions, the performance of the b-IrOx-based sensing system was analyzed by determining target antioxidants, including Trolox, GSH, AA, and caffeic acid. In Fig. 3A–D, the concentration-dependent absorption changes directly reflect the competitive reaction between TMB and antioxidants for •OH on the nanozyme surface: antioxidants scavenge •OH, reducing oxTMB formation and decreasing the 652 nm absorption intensity. This mechanism is further supported by the linear quantitative relationships in Fig. 3E–H, where both HAT-type (Trolox, caffeic acid) and SET-type (GSH, AA) antioxidants show reliable linear responses. Four linear calibration curves were obtained in the TMB-based colorimetric strategy (Table S1). The high R^2 values (>0.99) confirm the good linear relationship between ΔA and antioxidant concentration, laying a foundation for accurate quantitative detection. Additionally, selectivity studies Fig. S3 revealed that common interfering substances like glucose, amino acids, and various ions had negligible effects on the absorbance intensity, further ensuring the specificity of the b-IrOx nanozyme-based TMB colorimetric sensing system.

3.4. Real sample analysis

The practical applicability was confirmed through standard addition experiments on real food samples. NFC juices, including yellow peach juice, apple juice, and mango juice, were purchased from a local supermarket. In Fig. 4A and Table S2, for yellow peach juice, spiked Trolox at 10 μM, 20 μM, and 30 μM showed recoveries of 90.49%-101.78%. Apple juice exhibited recoveries of 98.97%-110.62% for the same spiked levels. Mango juice had recoveries of 99.62%-110.21%. All recoveries fell within the range of 90.49%-110.62%, and the relative standard deviations (RSD) for all measurements were less than 3%. These results indicate minimal matrix interference and validate that the detection system is reliable for real sample analysis.

To verify the practical applicability of the developed b-IrOx-based sensing system, this study determined the TAC of real samples (mango juice, yellow peach juice, apple juice) using the b-IrOx-based TMB colorimetric method. Commercial ABTS kit and FRAP kit were used as the reference standard, and the results were retained for accuracy comparison. All experiments used Trolox as the standard substance to ensure consistency in TAC quantification, with results expressed as μM TE. The TAC detection results of the two methods for each juice sample have been summarized in Fig. 4B and Table 1. These results confirm the reliability and consistency of the developed b-IrOx-based TMB colorimetric method, ABTS kit and FRAP kit in TAC measurement. Notably, the b-IrOx nanozyme, which exhibits POD-like activity and serves as the centerpiece of this innovative colorimetric approach, offers clear

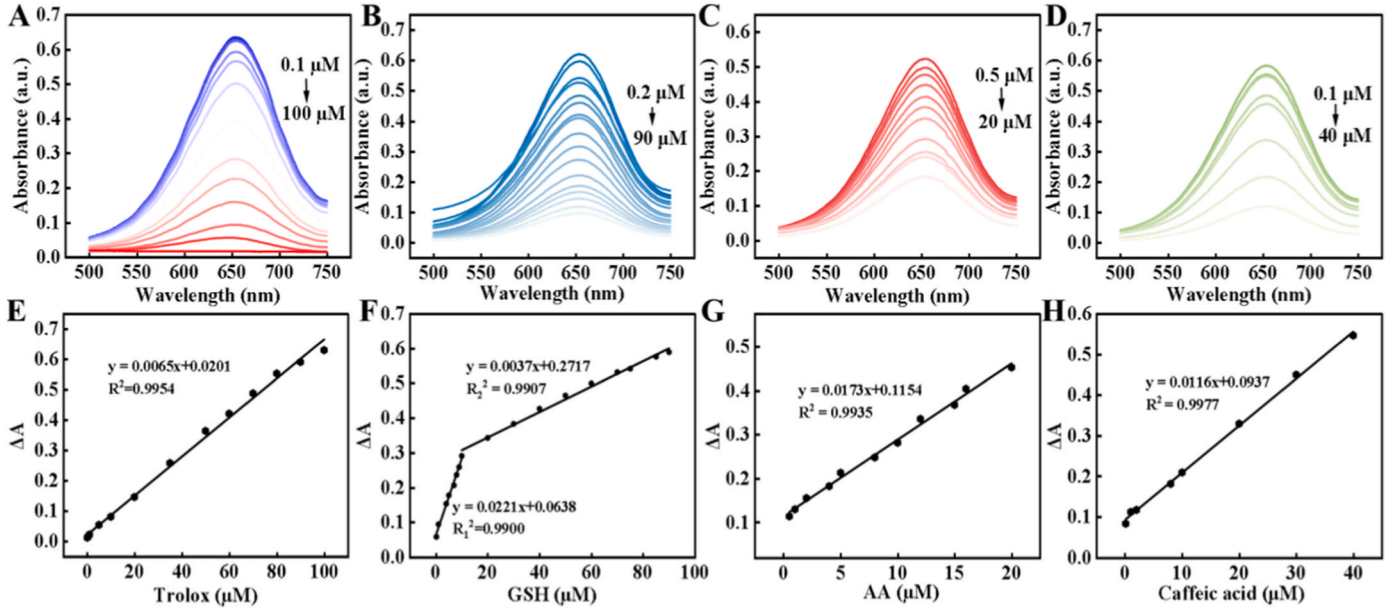


Fig. 3. Optical density values of the b-IrOx nanozyme-based sensing strategy as a function of HAT species antioxidants (A), Trolox and (D) caffeic acid, and SET working species antioxidants (B), GSH and (C) AA. (E-H) Linear calibration plots corresponding to (A-D) with TMB as the substrate, respectively.

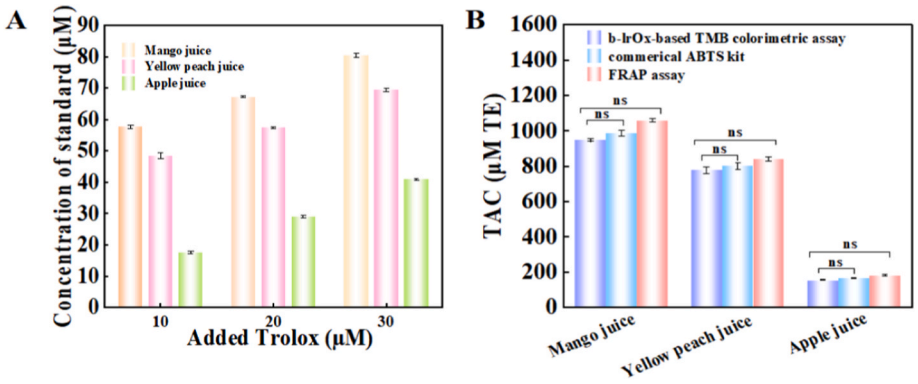


Fig. 4. (A), Repeatability (n = 3) measurements of the nanozyme-based assay for different Trolox standards recovery study in different fruit samples in TMB systems. (B), Comparison of TAC detection in three samples using the commercial ABTS kit, FRAP kit and the b-IrOx-based TMB based colorimetric assay. Data are shown as mean ± SD ((ns: $p > 0.05$, *$p < 0.05$, **$p < 0.01$, and ***$p < 0.001$).

Table 1
Comparative study of TAC detection in fruits using the proposed b-IrOx-based TMB colorimetric strategies and a standardized ABTS kit.

Samples	b-IrOx-based TMB colorimetric assay (μM, Mean ± SD)	ABTS kit (μM, Mean ± SD)	FRAP kit (μM, Mean ± SD)
Yellow peach juice	776.72 ± 2.47	801.10 ± 2.58	840.62 ± 12.32
Apple juice	154.77 ± 1.70	165.30 ± 2.24	181.81 ± 3.26
Mango juice	948.31 ± 0.83	987.03 ± 1.75	1059.13 ± 9.56

benefits compared to natural enzymes, including easy synthesis and improved stability. Compared to traditional POD-based commercial ABTS kits, the developed TMB colorimetric method shows comparable TAC detection capabilities for the tested fruit juices, while avoiding over-reliance on complex detection platforms.

Overall, the b-IrOx-based TMB colorimetric method presents a promising alternative for TAC detection and analysis in practical scenarios such as small-scale fruit juice processing plants and routine quality control. It maintains accuracy comparable to commercial ABTS kits and FRAP kits, providing a stable, easy-to-operate solution for TAC quantification in fruit juice samples.

4. Conclusion

This study successfully synthesized a novel b-IrOx nanozyme with intrinsic peroxidase-like activity via a one-step biomimetic mineralization strategy using BSA as a template. The as-prepared b-IrOx efficiently catalyzes the oxidation of TMB in the presence of H_2O_2 and generates hydroxyl radicals, enabling selective and sensitive colorimetric detection of TAC. The established b-IrOx-based colorimetric assay was applied to determine TAC in three commercial fruit juices, showing high accuracy with recoveries of 90.49%-110.62% and excellent reproducibility with RSD <3.0%. Comparative analysis with a commercial ABTS TAC kit revealed no statistically significant difference, validating the reliability and consistency of the proposed method. These results demonstrate that the b-IrOx-based colorimetric sensor provides a cost-effective, straightforward, and reliable alternative for rapid and accurate TAC quantification in food samples, holding great practical potential for routine quality control and on-site monitoring in food analysis.

CRediT authorship contribution statement

Shuangshuang Yan: Writing – original draft, Investigation. **Dongying An:** Writing – original draft, Validation, Data curation. **Yutian Zhou:** Visualization, Investigation. **Xinli Guo:** Visualization, Investigation. **Zhihang Qin:** Investigation. **Fangliang Yang:** Project administration, Investigation, Funding acquisition. **Yang Zhang:** Writing – review & editing, Supervision, Funding acquisition, Conceptualization.

Ethical statement

No coercion to participate, full disclosure of study requirements and risks, written or verbal consent of participants, no release of participant data without their knowledge, ability to withdraw from the study at any time.

Declaration of competing interest

The authors declare that they have no known competing financial interests or personal relationships that could have appeared to influence the work reported in this paper.

Acknowledgments

The authors appreciate financial supports from the Shenyang Science and Technology Talent Special Project (RC230022), Natural Science Foundation Joint Fund of Liaoning Province (2023-MSLH-288 and 2025-MSLH-668), Shenyang Medical College Project (SYKT2025004) and Science and Technology Innovation Fund Project of Shenyang Medical College (Y20250504).

Appendix A. Supplementary data

Supplementary data to this article can be found online at https://doi.org/10.1016/j.lwt.2026.119663.

Data availability

No data was used for the research described in the article.

References

Acidri, R., Sawai, Y., Sugimoto, Y., Handa, T., Sasagawa, D., Masunaga, T., et al. (2020). Phytochemical profile and antioxidant capacity of coffee plant organs compared to green and roasted coffee beans. *Antioxidants, 9*(2), 93. https://doi.org/10.3390/antiox9020093

Alshatteri, A. H., Ali, G. K., & Omer, K. M. (2023). Enhanced peroxidase-mimic catalytic activity via cerium doping of strontium-based metal–organic frameworks with design of a smartphone-based sensor for on-site salivary total antioxidant capacity detection in lung cancer patients. *ACS Applied Materials & Interfaces, 15*, 21239–21251. https://doi.org/10.1021/acsami.3c01007

Apak, R., Özyürek, M., Güçlü, K., & Çapanoğlu, E. (2016). Antioxidant activity/capacity measurement. 1. Classification, physicochemical principles, mechanisms, and electron transfer (ET)-based assays. *Journal of Agricultural and Food Chemistry, 64*, 997–1027. https://doi.org/10.1021/acs.jafc.5b04739

Baranwal, A., Polash, S., Aralappanavar, V., Behera, B., Bansal, V., & Shukla, R. (2024). Recent progress and prospect of metal–organic framework-based nanozymes in biomedical application. *Nanomaterials, 14*(3), 244. https://doi.org/10.3390/nano14030244

Çelik, E. E., Cömert, E. D., & Gökmen, V. (2024). The power of the quencher method in measuring total antioxidant capacity of foods: Importance of interactions between different forms of antioxidants. *Talanta, 269*, Article 125474. https://doi.org/10.1016/j.talanta.2023.125474

Chaudhary, M. R., Chaudhary, S., Sharma, Y., Singh, T. A., Mishra, A. K., Sharma, S., et al. (2023a). Aging, oxidative stress and degenerative diseases: Mechanisms, complications and emerging therapeutic strategies. *Biogerontology, 24*, 609–662. https://doi.org/10.1007/s10522-023-10050-1

Chen, X., Qi, Y., He, B., Liang, Y., Lei, Y., & Sun, J. (2023b). Fabrication of adjustable Au/Carbon hybrid nanozymes with photothermally enhanced peroxidase activity and ultra-sensitivity for glutathione detection. *ACS Applied Materials & Interfaces, 15*, 20788–20799. https://doi.org/10.1021/acsami.3c02420

Chen, Y., Zhang, Z., Ouyang, Y., Reheman, A., & Jiang, B. (2025). Enhanced peroxidase-like nanozyme: Copper-poly(tannic acid) for advanced colorimetric assay of total antioxidant capacity. *RSC Advances, 15*, 11401–11408. https://doi.org/10.1039/d5ra00995b

Demirci-Çekiç, S., Özkan, G., Avan, A. N., Uzunboy, S., Çapanoğlu, E., & Apak, R. (2022). Biomarkers of oxidative stress and antioxidant defense. *Journal of Pharmaceutical and Biomedical Analysis, 209*(4), Article 114477. https://doi.org/10.1016/j.jpba.2021.114477

Deshwal, A., Saxena, K., Sharma, G., Rajesh, Sheikh, F. A., Seth, C. S., et al. (2024). Nanozymes: A comprehensive review on emerging applications in cancer diagnosis and therapeutics. *International Journal of Biological Macromolecules, 256*(pt 1), Article 128272. https://doi.org/10.1016/j.ijbiomac.2023.128272

Duarte, R. M. B. O., Brandão, P. F., & Duarte, A. C. (2023). Multidimensional chromatography in environmental analysis: Comprehensive two-dimensional liquid versus gas chromatography. *Journal of Chromatography A, 1706*, Article 464288. https://doi.org/10.1016/j.chroma.2023.464288

Egu, S. A., Ali, I., Khan, K. M., Chigurupati, S., Qureshi, U., Salar, U., et al. (2022). Syntheses, in vitro, and in silico studies of rhodanine-based schiff bases as potential α-amylase inhibitors and radicals (DPPH and ABTS) scavengers. *Molecular Diversity, 27*, 767–791. https://doi.org/10.1007/s11030-022-10454-0

Forman, H. J., & Zhang, H. (2021). Targeting oxidative stress in disease: Promise and limitations of antioxidant therapy. *Nature Reviews Drug Discovery, 20*, 689–709. https://doi.org/10.1038/s41573-021-00233-1

Han, X., Liu, L., Gong, H., Luo, L., Han, Y., Fan, J., et al. (2022). Dextran-stabilized fe-mn bimetallic oxidase-like nanozyme for total antioxidant capacity assay of fruit and vegetable food. *Food Chemistry, 371*, Article 131115. https://doi.org/10.1016/j.foodchem.2021.131115

Ishida, H., Yamasaki, N., Otsuka, Y., Mori, D., Shimamura, T., Hasegawa, T., et al. (2022). Electrochemical antioxidant capacity measurement: A downsized system and its application to agricultural crops. *Analytical Sciences, 38*, 151–156. https://doi.org/10.2116/analsci.21P217

Jelic, M. D., Mandic, A. D., Maricic, S. M., & Srdjenovic, B. U. (2021). Oxidative stress and its role in cancer. *Journal of Cancer Research and Therapeutics, 17*, 22–28. https://doi.org/10.4103/jcrt.JCRT_862_16

Li, J., Li, Y., Shi, Y., Li, Z., Deng, C., Zhang, G., Zhou, Q., Wang, Z., & Yu, X. (2025). Fluorescence/colorimetric intelligent sensor based on Fe-adsorbing carbon dots nanozymes for selective recognition and quantification of total antioxidant capacity in foods and cells. *Food Chemistry, 490*. https://doi.org/10.1016/j.foodchem.2025.145052

Li, H., Zhai, B., Sun, J., Fan, Y., Zou, J., Cheng, J., et al. (2021). Antioxidant, anti-aging and organ protective effects of total saponins from aralia taibaiensis. *Drug Design, Development and Therapy, 15*, 4025–4042. https://doi.org/10.2147/dddt.S330222

Liang, M., & Yan, X. (2019). Nanozymes: From new concepts, mechanisms, and standards to applications. *Accounts of Chemical Research, 52*, 2190–2200. https://doi.org/10.1021/acs.accounts.9b00140

Mou, X., Wu, Q., Zhang, Z., Liu, Y., Zhang, J., Zhang, C., et al. (2022). Nanozymes for regenerative medicine. *Small Methods, 6*(11), Article 2200997. https://doi.org/10.1002/smtd.202200997

Munteanu, I. G., & Apetrei, C. (2021). Analytical methods used in determining antioxidant activity: A review. *International Journal of Molecular Sciences, 22*(7), Article 338022. https://doi.org/10.3390/ijms22073380

Nakano, Y., Biegasiewicz, K. F., & Hyster, T. K. (2019). Biocatalytic hydrogen atom transfer: An invigorating approach to free-radical reactions. *Current Opinion in Chemical Biology, 49*, 16–24. https://doi.org/10.1016/j.cbpa.2018.09.001

Niu, P. B., Wang, Y. Q., Hu, R., & Yang, T. (2024). Cu nanoparticles/CoO/carbon nanofibers as an enhanced peroxidase mimic for total antioxidant capacity assessment in drinks. *ACS Applied Nano Materials, 7*, 5996–6004. https://doi.org/10.1021/acsanm.3c05920

Possa, L.d. O., Hinkelman, J. V., Santos, C. A.d., Oliveira, C. A.d., Faria, B. S., Hermsdorff, H. H. M., et al. (2021). Association of dietary total antioxidant capacity with anthropometric indicators, c-reactive protein, and clinical outcomes in hospitalized oncologic patients. *Nutrition, 90*, Article 111359. https://doi.org/10.1016/j.nut.2021.111359

Rumpf, J., Burger, R., & Schulze, M. (2023). Statistical evaluation of DPPH, ABTS, FRAP, and Folin-Ciocalteu assays to assess the antioxidant capacity of lignins. *International Journal of Biological Macromolecules, 233*, Article 123470. https://doi.org/10.1016/j.ijbiomac.2023.123470

Sánchez-Martín, V., Morales, P., González-Porto, A. V., Iriondo-DeHond, A., López-Parra, M. B., Del Castillo, M. D., et al. (2022). Enhancement of the antioxidant capacity of thyme and chestnut honey by addition of bee products. *Foods, 11*(19), 3118. https://doi.org/10.3390/foods11193118

Teleanu, D. M., Niculescu, A.-G., Lungu, I. I., Radu, C. I., Vladâcenco, O., Roza, E., et al. (2022). An overview of oxidative stress, neuroinflammation, and neurodegenerative diseases. *International Journal of Molecular Sciences, 23*, 5938. https://doi.org/10.3390/ijms23115938

Velusamy, P., Mohan, T., Ravi, D. B., Kishore Kumar, S. N., Srinivasan, A., Chakrapani, L. N., et al. (2020). Targeting the Nrf2/are signalling pathway to mitigate isoproterenol-induced cardiac hypertrophy: Plausible role of hesperetin in redox homeostasis. *Oxidative Medicine and Cellular Longevity, 2020*, 1–13. https://doi.org/10.1155/2020/9568278

Yalçın, S., Karakaş, Ö., Okudan, E.Ş., Başkan, K. S., Çekiç, S. D., & Apak, R. (2021a). HPLC detection and antioxidant capacity determination of brown, red and green algal pigments in seaweed extracts. *Journal of Chromatographic Science, 59*, 325–337. https://doi.org/10.1093/chromsci/bmaa107

Yang, W., Yang, X., Zhu, L., Chu, H., Li, X., & Xu, W. (2021b). Nanozymes: Activity origin, catalytic mechanism, and biological application. *Coordination Chemistry Reviews, 448*, Article 214170. https://doi.org/10.1016/j.ccr.2021.214170

Zeb, A. (2020). Concept, mechanism, and applications of phenolic antioxidants in foods. *Journal of Food Biochemistry, 44*(9), Article e13394. https://doi.org/10.1111/jfbc.13394

Zhang, Q., Su, G., Yang, Q., Wei, Z., Wang, J., Zheng, L., et al. (2021). Round scad-derived octapeptide WCPFSRSF confers neuroprotection by regulating Akt/Nrf2/NFkB signaling. *Journal of Agricultural and Food Chemistry, 69*, 10606–10616. https://doi.org/10.1021/acs.jafc.1c04774

Zhang, X., Wang, J., Chang, N., Yang, Y., Li, Y., Wei, Q., et al. (2024). Cu-BTC derived mesoporous CuS nanomaterial as nanozyme for colorimetric detection of glutathione. *Molecules, 29*(9), 2117. https://doi.org/10.3390/molecules29092117